# Investigating the origin of the high photoconductivity of rubrene single crystals

Hikmat Najafov, Byunggook Lyu, and Ivan Biaggio
*Department of Physics, Lehigh University, Bethlehem, Pennsylvania 18015, USA*

Vitaly Podzorov
*Department of Physics and Astronomy, Rutgers University, Piscataway, New Jersey 08854, USA*
(Received 29 May 2007; revised manuscript received 11 December 2007; published 6 March 2008)

The rubrene molecular crystal has the unique property of showing a strong photoconductivity for light wavelengths that are close to the absorption edge. We studied the microsecond dynamics of the photoconductivity induced by short light pulses to characterize the way in which photoinduced excitons efficiently ionize to produce free charge carriers. We found that the photoconductivity is produced by carriers released after an average time of 100 $\mu$s from a "reservoir state" that originates from the photoexcited molecular excitons. The conversion of photoexcited excitons into this reservoir state happens only at the surface of the crystal within a depth of the order of a few micrometers, but in this region close to the surface, a photoexcited molecular exciton has a probability of the order of unity to ultimately lead to a mobile charge carrier. This high carrier photoexcitation efficiency leads to a pronounced shortening of the photocurrent rise time for decreasing wavelength or increasing energy of the excitation pulses because of the effect of quadratic recombination of the photocarriers.

DOI: 10.1103/PhysRevB.77.125202 PACS number(s): 72.20.Jv, 31.70.Ks, 72.40.+w, 71.35.−y

## I. INTRODUCTION

The physical process by which an absorbed photon may photoexcite mobile charge carriers in a pure single crystal is fundamentally different, compared to standard covalently bound semiconductors, when the crystal consists of large molecules bound only by van der Waals attraction, as is often the case in organic molecular crystals. At a fundamental level, one expects that the weak intermolecular interaction leads to a weak overlap of the electron wave functions between neighboring molecules, which in very general terms tends to decrease the probability that a molecule in an excited state transfers its electron to a neighboring molecule to generate a delocalized electron and hole pair. Instead, the probability for electron transfer to a neighboring molecule could remain significantly lower than the probability for the molecule to return to its ground state by either radiative or nonradiative recombination. In other words, in van der Waals bound molecular crystals, one expects that photoexcitation mostly leads to localized molecular excitons that only rarely autoionize to produce free carriers, leading to a small photoconductivity even when the optical absorption becomes very high.[1–3]

In some cases, however, and in contrast to the above expectations, a signal that can be assigned to free charge carriers has been observed within a fraction of a picosecond from photon absorption,[4–6] and there has been a lively discussion in the literature about the nature of photoexcitation in molecular materials and the possibility that photon absorption can directly lead to the creation of delocalized mobile carriers.[7–12] The discussion is farther complicated by the variety of excitonic states that are found in organic materials.[1–3,12–16]

In this context, we have recently investigated the photoexcitation mechanism in rubrene single crystals.[17] By varying the energy of the incident photons, we observed how, initially, photon absorption leads to the promotion of the ground state electron onto one of the vibronic sublevels of the first electronic excited state of the rubrene molecule, thus creating the molecular exciton equivalent of a Frenkel exciton.[17] This exciton subsequently decays within a few nanoseconds, leading to a fast photoluminescence signal. Finally, a large *delayed* photoconductivity grows from zero with a buildup time of up to 100 $\mu$s after photoexcitation.[17] We assigned this delayed photoconductivity to the decay of an unknown intermediary state (a "reservoir") that was populated from the initial photoexcited exciton, a conclusion that was derived mainly from the correspondence between the excitation spectrum of the photocurrent and the excitation spectrum of the luminescence.[17] In the following, we will use the term *reservoir* to describe this as yet unspecified intermediary state that slowly releases free carriers, thus leading to both a slowly rising and a long-lived photoconductivity after pulsed excitation.

In this work, we investigate the dependence of the photoconductivity dynamics in rubrene single crystals from the photon energy, photon density, and temperature. We develop a general model applicable to any case where a pulsed excitation results in a localized state that can ionize into free charge carriers. We use the model to analyze the evolution of the photoconductivity in rubrene after exposure to a 20 ps long laser pulse, which allows us to separate the processes of exciton creation, transfer to the reservoir state, and carrier generation, because they occur on different time scales. From this, we obtain information on the reservoir state and on the properties of the photoexcited carriers.

Recently, it has been pointed out that oxygen-related defects close to the surface of rubrene play an important role in light-induced switching of field-effect transistors[18] and in the photoluminescence.[19] One of the conclusions we will arrive at is that the intermediary reservoir state mentioned above could be the result of an exciton interacting with such an oxygen-related defect state to create a bound state from which holes are later thermally excited. We will also show

 

that the spectral dependence of the photoconductivity rise time that we observed in Ref. 17 can be assigned to the spectral dependence of the excitation density and the influence of quadratic recombination of the photoexcited charge carriers. This fact will allow us to explain both the wavelength and the power dependence of the photoconductivity and to use the temperature dependence of the buildup time of the photoconductivity to estimate the activation energy of the process that leads—over the long-lived reservoir state we identified—from the molecular exciton to a delocalized mobile charge carrier.

In the following, we first present a simple physical model of photoexcitation that can be used to account for most of the experimental observations. Next, we present the typical photocurrent dynamics observed in rubrene single crystals at room temperature and interpret its dependence from the laser pulse energy and from the wavelength in view of the model. Finally, we will discuss the temperature dependence of the photoconductivity dynamics in different power regimes. The experiments and their interpretation in view of the model will allow us to paint a more complete physical picture of the processes that lead from the initial photoexcitation to a bound molecular exciton and ultimately to delocalized, mobile charge carriers.

## II. THEORETICAL MODEL

We want to describe the time evolution of a photoexcited carrier density after short-pulse photoexcitation with a pulse length that is much shorter than any of the relevant subsequent time dependences. We assume that one type of carrier has a significantly larger mobility lifetime product than the other one, and without loss of generality we assume these carriers to be holes with a density $p(t)$ (we know that holes have the largest mobility in rubrene crystals[20]). We assume that the photoexcitation results in the filling of an intermediary state (the reservoir mentioned above) with a density $N_R(t)$, from which holes are released with a rate $w$.

It should be noted that the model we are about to present and the approximate analytical expressions that we will develop for describing the photoconductivity transients are valid, in general, for any experiment where a pulsed excitation results in the creation of a localized state that can ionize into free charge carriers. From the point of view of the model, the reservoir state that we are studying here is indistinguishable from a long-lived exciton.

After holes are released from the reservoir, they can recombine back into the electrons that they have left behind, with a rate determined by a (quadratic) recombination constant $\gamma$. In addition, we also allow for the holes to be trapped in a state $N_T$, with an efficiency given by a constant $\gamma_T$. This is required in order to make the model general enough, and it represents a free-hole lifetime that would be observed for a hole independently of the way it has been created.

The resulting system of equations is

$$\frac{dp}{dt} = -p^2\gamma - p\gamma_T N_T + wN_R, \tag{1}$$

$$\frac{dN_R}{dt} = -wN_R. \tag{2}$$

We will use this model to describe the delayed photocurrent that we observe in rubrene after short-pulse excitation. The appropriate initial conditions immediately after illumination with the photoexcitation pulse at $t=0$ are $p(0)=0$ and $N_R(0)>0$. This is justified by the fact that in rubrene the dark conductivity is negligible compared to the photoconductivity amplitude, and by the fact that, for most of the pulse energy and wavelength range we investigated, we did not observe any significant immediate release of charge carriers at $t=0$. The density $p(t)$ increases from zero, reaches a maximum, and decays back to zero.

The model implies that the density $N_R(t)$ decreases exponentially, as $N_R(t)=N_R(0)\exp(-wt)$. The assumption here is clearly that the only way in which the reservoir state can decay is through carrier excitation. Even though it would be possible to include another decay mechanism for $N_R(t)$ by adding a term to the right-hand side of Eq. (2), we find that this does not add in a useful way to the discussion of this model and the interpretation of our results later.

In the following, we first overview the photoexcitation dynamics in several useful physical limits, and then we will give analytical approximations to the full solution of Eqs. (1) and (2) that will be useful to discuss the dependence of the observed photoconductivity amplitude and buildup rate on the energy of the illuminating laser pulse.

The relationship between the magnitudes of the carrier release rate $w$ and of the linear trapping rate $\gamma_T N_T$ determines two distinct regimes where different physical mechanisms are responsible for a similar photocurrent dynamics characterized by a buildup from zero and a relaxation back to zero with a longer relaxation time. In the *slow-photoexcitation regime*, the buildup rate and decay rate at low exposure are given by $w$ and $\gamma_T N_T$, respectively, while it is the other way around in the *fast-photoexcitation regime*. In addition, the amount of excitation stored in the reservoir, $N_R(0)$, determines a *low-exposure limit* [small $N_R(0)$] and a *high-exposure limit* [large $N_R(0)$].

For the fast-photoexcitation regime, $w \gg \gamma_T N_T$, and $p(t)$ reaches a maximum when either the reservoir has basically emptied itself (in the low-exposure limit) or when the excitation rate becomes compensated by the quadratic-recombination rate (high-exposure limit). In the first case, the maximum is reached at a time $t_{\max}$ when $N_R(t_{\max})$ is significantly lower than $N_R(0)$. In the second case, the maximum is reached before the reservoir has significantly emptied itself and $N_R(t_{\max}) \approx N_R(0)$. An extreme example of the fast-photoexcitation regime is encountered for very large release rates $w$, practically corresponding to an impulsive creation of charge carriers, which is then followed by a decay of their density, with either a quadratic-recombination behavior (high exposure) or a linear recombination behavior (a simple exponential decay observed at low exposure) depending on the initial carrier density. In this example, the fast excitation sets up an initial condition for a subsequent evolution, and while later dynamics can be more complicated, the peak am-

plitude depends linearly on the total density of carriers released from the reservoir.

For the slow-photoexcitation regime, $w \ll \gamma_T N_T$, and $p(t)$ reaches a maximum when the excitation rate becomes compensated by either the linear recombination rate [low exposure or small $N_R(0)$] or by the quadratic-recombination rate [high exposure or large $N_R(0)$]. In both cases, the maximum is reached before the reservoir has significantly emptied itself and $N_R(t_{\max}) \approx N_R(0)$ is always valid.

In the fast-photoexcitation regime of $w \gg \gamma_T N_T$ and in the low-exposure limit where $\gamma N_R(0) \ll w$, the photocarrier density basically grows exponentially with a rate $w$ and reaches a maximum amplitude of

$$p_{max} \approx N_R(0). \tag{3}$$

For all other cases (fast photoexcitation and high exposure or all limits of slow photoexcitation), the maximum of $p(t)$ is reached when the reservoir has not significantly emptied itself, and a simple expression for the maximum amplitude $p_{max}=p(t_{max})$ can be obtained by setting to zero the time derivative in Eq. (1) and assuming $N_R(t_{max})=N_R(0)$,

$$p_{max} = \frac{\gamma_T N_T}{2\gamma}\left[\sqrt{1+\frac{4\gamma w N_R(0)}{\gamma_T^2 N_T^2}} - 1\right]. \tag{4}$$

The high-exposure limit corresponds to $N_R(0) \gg w/\gamma$ for fast photoexcitation and to $N_R(0) \gg \gamma_T^2 N_T^2/(\gamma w)$ for slow photoexcitation. In both cases the maximum amplitude of the photocarrier density tends to

$$p_{max} \approx p_1 = \sqrt{\frac{w N_R(0)}{\gamma}}, \tag{5}$$

with a buildup rate that depends on $N_R(0)$.

The low-exposure limit for slow photoexcitation corresponds to $N_R(0) \ll \gamma_T^2 N_T^2/(\gamma w)$. The amplitude of photocarrier density then tends to

$$p_{max} \approx \frac{w N_R(0)}{\gamma_T N_T}, \tag{6}$$

and the buildup time tends to $(\gamma_T N_T)^{-1}$. We see that in both the fast-photoexcitation and the slow-photoexcitation regimes, the photocurrent amplitude varies linearly with $N_R(0)$ at low exposures [Eqs. (3) and (6)] and becomes proportional to the square root of $N_R(0)$ at high exposures, when quadratic recombination becomes important.

As an example, the high- and low-photoexcitation limits for the slow-photoexcitation case are typically observed when a semiconductor is exposed to an intense (dominant quadratic recombination) or to a weak (dominant linear recombination) above band-gap continuous wave illumination.[21,22] In the present case, the role of the above band-gap illumination is played by the long-lived reservoir state, whose initial density is directly related to the energy density in the laser pulse that fills it at $t=0$. The limit of continuous excitation is obtained when $w \to 0$ while $wN_R(0)$ is held constant.

Besides the peak photocurrent amplitude, we also need to quantify the variation of the photocurrent buildup time with the initial reservoir density $N_R(0)$. In the high-exposure limit, quadratic recombination affects the buildup rate of the photocarrier density, which then becomes dependent on $N_R(0)$. The easiest way to show this is for the case when linear recombination is negligible. The limit of Eq. (1) for $N_T \to 0$ is

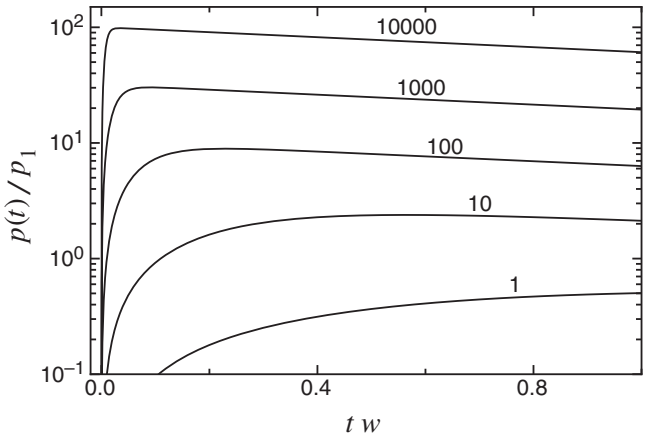


FIG. 1. Prediction of Eq. (10) in the normalized case of "$w=\gamma=1$" and the various values of $\gamma N_R(0)$ shown.

$$\frac{dp}{dt} = -p^2\gamma + wN_R(t). \tag{7}$$

When $N_R(0)$ is so large that the quadratic-recombination term already stops the buildup significantly before the reservoir has had the time to empty itself, we can use $N_R(t) \approx N_R(0)$ to find the simple solution

$$p(t) = p_1 \tanh[\sqrt{N_R(0)w\gamma}t], \tag{8}$$

with a nonexponential buildup time of $(N_R(0)w\gamma)^{-1/2}$ and an amplitude $p_1$ given by Eq. (5).

We can also derive more general approximate analytical solutions for the time evolution of the hole density $p(t)$. While above we only discussed the limiting behaviors at low and high exposures, these expressions allow us to study when the deviation from the low-exposure behavior starts as a function of $N_R(0)$. The first expression can be derived for the case when linear recombination is negligible, and it is a general solution of Eqs. (2) and (7) for $\gamma_T N_T=0$ that is valid both for low exposure and for high exposure,

$$N_R(t) = N_R(0)e^{-wt}, \tag{9}$$

$$p(t) = p_1 e^{-wt/2}\frac{K_1(\xi e^{-wt/2}) - \beta I_1(\xi e^{-wt/2})}{K_0(\xi e^{-wt/2}) + \beta I_0(\xi e^{-wt/2})}, \tag{10}$$

where $\xi=2\sqrt{N_R(0)\gamma/w}$ and $\beta=K_1(\xi)/I_1(\xi)$. Here, $I_m$ and $K_m$ are the modified Bessel functions of the first and of the second kind, of real order $m$. This solution describes the full dynamics of the photocarrier density all the way from the low-exposure to the high-exposure limit. An example of a plot of the above equation for $w=\gamma=1$ and $N_R(0)=1,10,100,1000,10\,000$ is shown in Fig. 1. A longer solution based on Bessel and gamma functions can also be found

for the full system of Eqs. (1) and (2) including the linear recombination term, but its analytical form is too complicated to be useful in this work.

We now need to analyze the predictions of this model when $\gamma_T N_T > 0$. The solution described by Eq. (10) is of limited usefulness because it does not take into account any relaxation mechanism other than direct electron-hole recombination. Even though it is technically in the fast-photoexcitation limit, it does not give a complete picture and can only be used to analyze the time dependence on the shorter time scale where the buildup is seen.

For the more general case where $\gamma_T N_T > 0$, we derived two useful analytical expressions that describe the low-exposure behavior and the initial deviations as $N_R(0)$ increases. These two expressions are valid for the slow-photoexcitation and for the fast-photoexcitation case, respectively.

For the slow-photoexcitation case, $w \ll \gamma_T N_T$, we find

$$p(t) = \frac{wN_R(0)}{\gamma_T N_T} \frac{F(t)}{1 + \kappa[1 - F(t)]}, \tag{11}$$

where $\kappa = \gamma w N_R(0)/(\gamma_T N_T)^2$ and $F(t) = \exp(-wt) - \exp(-\gamma_T N_T[1+\kappa]t)$. This expression is valid as long as $\kappa$ is of the order of 1 or less, so that it is only applicable in the low-exposure regime and for the initial deviation from it. As expected, the buildup rate is given by $\gamma_T N_T$ at low exposure, corresponding to the hole lifetime. As $N_R(0)$ increases, the buildup rate becomes $\gamma_T N_T(1+\kappa)$, initially deviating linearly from the low-exposure value. At the same time, the denominator in Eq. (11) starts increasing and the maximum magnitude of $p(t)$ becomes sublinear with $N_R(0)$.

For the fast-photoexcitation case, $w \gg \gamma_T N_T$, we find[25]

$$p(t) = N_R(0) \frac{e^{-\gamma_T N_T t} - e^{-wt}}{1 + H(t) - G(t)}, \tag{12}$$

where $G(t) = \gamma N_R(0) w^{-1}[1 - \exp(-wt)]$ and $H(t) = \gamma N_R(0) \gamma_T^{-1} N_T^{-1}[1 - \exp(-\gamma_T N_T t)]$. This expression is valid as long as $\gamma N_R(0)$ remains smaller than $w$. The buildup rate at low exposure is given by $w$. As $N_R(0)$ increases, the buildup is affected by the $H(t) - G(t)$ term in the denominator, which grows from zero and becomes of the order of $\gamma N_R(0)/w$ for times near $1/w$. This leads to both a shortening of the buildup time and to a reduction of the maximum amplitude when $\gamma N_R(0) \approx w$, which marks the transition to the high-exposure regime from the point of view of buildup rate and maximum amplitude. This can also be seen by neglecting $G(t)$, linearizing the exponential in $H(t)$ at times much shorter than $\gamma_T^{-1} N_T^{-1}$, and then recontracting the denominator into an exponential of $\gamma N_R(0) t$. One then obtains a buildup rate of $w + \gamma N_R(0)$, which deviates linearly from the low-exposure value and doubles in correspondence to the condition $\gamma N_R(0) \approx w$. The amplitude of the final exponential relaxation with decay rate $\gamma_T N_T$, however, starts being affected by an increasing $N_R(0)$ already at the much smaller values when $H(t = \gamma_T^{-1} N_T^{-1}) \approx 1$, that is, when $\gamma N_R(0)$ starts becoming comparable to $\gamma_T N_T$. The amplitude of the final relaxation essentially determines the integral of the photocurrent signal when $w \gg \gamma_T N_T$. We can thus, in general, expect that in this fast-photoexcitation regime, the integral of the photocurrent starts saturating at exposures that are lower by a factor of $\gamma_T N_T w^{-1}$ with respect to the start of the saturation in the buildup rate.

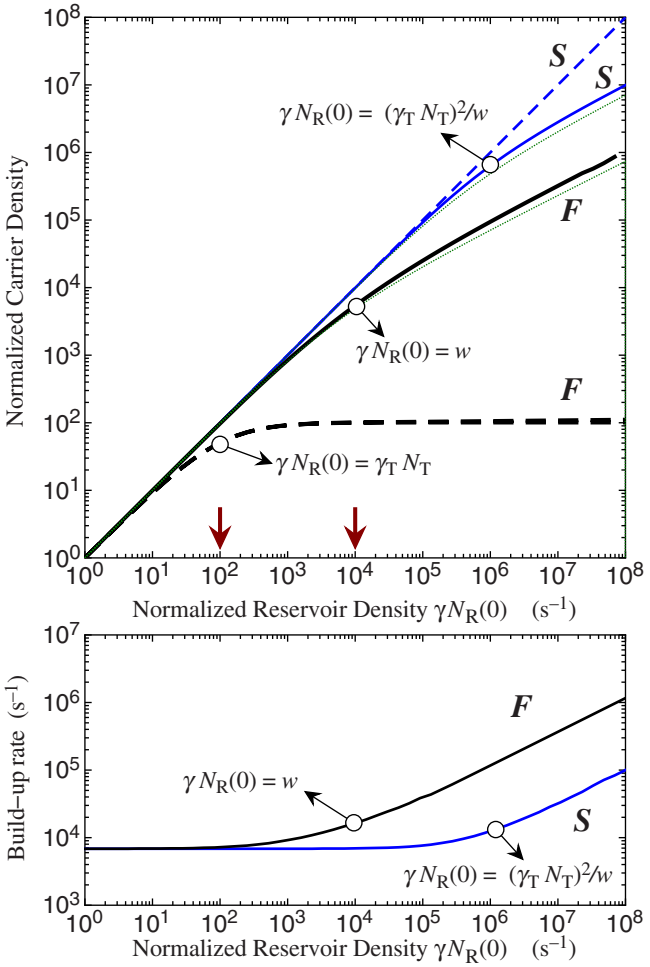


FIG. 2. (Color online) Numerical solution of the model [Eqs. (1) and (2)] for the dependence of the photoconductivity transient on the initial number of filled reservoir states $N_R(0)$. The upper graph shows the peak photocurrent amplitude (solid curves) and the amplitude of the final exponential decay (dashed curves) normalized to the same value for small $N_R(0)$. The lower graph shows the buildup rates calculated from the time needed to reach 80% of the peak amplitude. All curves are labeled with *S* and *F*, indicating the fast-photoexcitation regime and the slow-photoexcitation regime, respectively. The thin dotted lines are the approximations of Eqs. (11) and (12) for the peak amplitude. The curves for peak amplitude and buildup rate all tend toward a square-root dependence from $N_R(0)$ for large $N_R(0)$. The parameters used for the calculations were $w = 100\ s^{-1}$ and $\gamma_T N_T = 10^4\ s^{-1}$ for the slow-photoexcitation case, and vice versa for the fast-photoexcitation case. The arrows indicate these values on the $\gamma N_R(0)$ axis. The white circles mark the approximate conditions discussed in the text for which the transition from low exposure to high exposure takes place.

Figure 2 shows how the peak amplitude, the buildup rate, and the amplitude of the final exponential decay depend on the initial filling of the reservoir $N_R(0)$ for the case where $\gamma_T N_T$ and $w$ differ by 2 orders of magnitude (which corre-

sponds to the experimental observation in rubrene). The figure visualizes the limits discussed in the previous paragraph. The point at which the buildup rate starts accelerating is by 2 orders of magnitude smaller for the fast-photoexcitation regime than for the slow-photoexcitation regime, reflecting the different carrier-density dependent demarcation conditions in the two regimes, which are $\gamma N_R(0) \approx w$ and $\gamma N_R(0) \approx (\gamma_T N_T)^2/w$, respectively.

The saturation of the amplitude of the final exponential decay of the carrier density with exposure is a characteristic of the fast-exposure regime and does not occur at all in the slow-exposure regime. In the slow-exposure regime, the carrier density at long times becomes small enough that quadratic recombination does not play a role anymore and the carrier density is then given just by the equilibrium of excitation and recombination, $p(t) \approx w N_R(t) \gamma_T^{-1} N_T^{-1}$. Since $N_R(t) = N_R(0)\exp(-wt)$ in any case, the charge carrier density at long times will keep growing linearly with $N_R(0)$.

## III. EXPERIMENTS AND DISCUSSION

In the following, we first discuss the dependence of the observed photoconductivity transient on the energy and the wavelength of the illuminating pulses. We will then use the insights derived from these observations to interpret additional temperature dependent measurements of the photoconductivity and of the photoluminescence.

To determine the dynamics of the photocarrier density in rubrene, we illuminated a 1 mm thick crystal with 20 ps long laser pulses at a repetition rate of 10 Hz. A constant voltage of 315 V was applied to two 2 mm long silver contacts painted on the surface and spaced 2.2 mm apart along the *b* axis of the crystal. The illuminated area of 0.2 $mm^2$ was in the middle between the contacts. These contacts have been previously found to provide nearly Ohmic current-voltage characteristics in rubrene,[23] and the rubrene crystal has a high resistivity in the dark. We expect an essentially uniform electric field between contacts. We observed that the photocurrent dynamics does not depend on the interelectrode distance or the applied field, and that the peak photocurrent amplitude is much larger than the dark current even for electrodes 1 cm apart with a submillimeter illuminated spot in the middle. Varying the position of the illuminated spot between the electrodes has no influence on the photocurrent dynamics or amplitude. In addition, we did not see any change in photocurrent dynamics when decreasing the repetition rate of the laser by 1 order of magnitude, proving that our experiment is essentially a "single-shot" experiment. In general, we did not observe any dependence of the photocurrent dynamics from previous history in applied field, laser pulse energy, or wavelength.

Photocurrent traces were collected for different wavelengths between 585 and 530 nm and for different pulse fluences from 15 $\mu J/cm^2$ to 9 $mJ/cm^2$ with a 2 GHz sampling oscilloscope and averaged 150 times.

Examples of the typical photocurrent dynamics observed in rubrene under these circumstances are given in Fig. 3. A prominent feature of the photocurrent is that at low exposures, it starts appearing a long time of the order of 0.1 ms after the 20 ps long pulse illuminated the crystal:[17] the excitation remains stored in an intermediary localized state for several tens of microseconds before free carriers that can contribute to the photoconductivity appear. A second important feature is that the onset of the photoconductivity becomes faster at higher illuminating pulse energies and at shorter wavelengths.[17] Only at the highest exposures did we also observe what appears to be a small instantaneous photocurrent. This contribution does not affect the measurements presented here, and we will discuss it in detail in a future publication. In all our present measurements, the photocurrent corresponding to this different photocarrier generation mechanism remained relatively small (less than 10% of the delayed contribution even at the highest exposures) and did not otherwise affect the photocurrent dynamics in the microsecond and millisecond time scales, which is the subject of the present work. After having reached a maximum at a time in the microsecond region that depends on both pulse energy and wavelength, the photoconductivity relaxes with an exponential decay time (not visible in Fig. 3) that remains of the order of 10 ms, with no relevant dependence from the illuminating pulse energy or the wavelength.

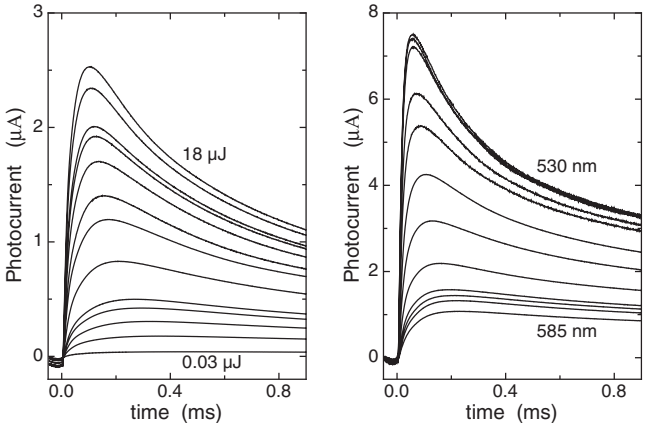


FIG. 3. Photocurrent dynamics observed in a rubrene single crystal after illumination with a 20 ps long pulse at 580 nm. The plot on the left shows traces obtained at various pulse energies from 0.03 to 18 $\mu$J. The illuminated area was $2 \times 10^{-3}$ $cm^{-2}$. The plot on the right shows traces obtained at various wavelengths for an illuminating pulse energy of 1.4 $\mu$J. The wavelength for each trace was from 585 to 530 nm in steps of 5 nm. The illuminated area was about $4 \times 10^{-4}$ $cm^{-2}$.

### A. Dependence on pulse energy

Several insights can be obtained by analyzing both the amplitude and rise time of the photocurrent curves in relation to the physical model presented in the previous section. Since the absolute amount of photoconductivity that can be obtained in a rubrene crystal is quite extraordinary, we start by assessing a lower limit to the quantum efficiency with which a photon is ultimately converted into a free carrier. This can be done because we localize the photoexcitation in time and observe the evolution of the photocurrent in the dark. In the optimum case where a single carrier drifts by the whole distance between the contacts (which is not the case in

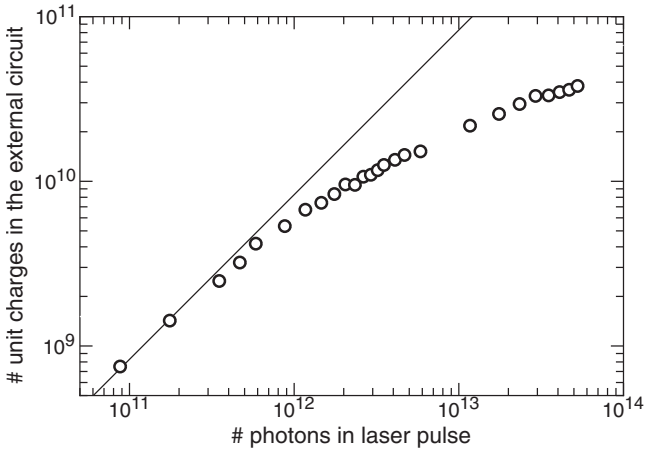


FIG. 4. Total charge flowing in the external circuit, expressed as number of unit charges, vs the total number of photons in the illuminating pulse. The wavelength of the pulse was 580 nm. The solid line gives a linear dependence.

our experiment), a single photoexcitation would lead to a single unit charge moving from one contact to the other through the external circuit. If the drift length $\ell_E$ is shorter than the interelectrode distance $d$, then a single photoexcitation will produce $\sim \ell_E/d$ unit charges in the external circuit. Hence, one can simply estimate the quantum efficiency $\eta$ by comparing the integral of the photocurrent to the total number of photons in the laser pulse,

$$\eta = \frac{d}{\ell_E}\frac{1}{eN_{ph}}\int_0^\infty I(t)dt, \tag{13}$$

where $e$ is the unit charge and $N_{ph}=E_p/(h\nu)$ is the number of photons in the illuminating pulse, with $E_p$ as the pulse energy. $I(t)$ is the magnitude of the photocurrent. Figure 4 plots the integrated photocurrent, expressed as a number of unit charges, against the number of photons in the laser pulse. The data points at the lowest exposure deliver $\eta\ell_E/d \approx 0.01$. The real quantum efficiency will be larger than this value because in the experiment of Fig. 4, the integral of the photocurrent is still growing with the applied field. From the absence of any variation of the photoconductivity dynamics with the applied field, we also know that the drift length is significantly shorter than the interelectrode spacing. In any case, the lower limit of 0.01 already hints at a quantum efficiency for free-carrier photoexcitation that is extraordinarily large for an organic material. We will discuss its possible origin below after we have presented some additional analysis of the photoconductive properties of rubrene.

Another feature readily observed from Fig. 4 is that the data points at the higher exposure deviate from a linear dependence. This is caused by the effect of quadratic recombination on the carrier density, so that the pulse energy at which the deviation starts depends on the optical energy density in the illuminated area. We will prove this interpretation with several observations in the following, where we will analyze the power and wavelength dependence of the photocurrent amplitude and of its buildup rate. These two quantities are extracted from the data by fitting the buildup dynamics with a time dependence of the kind $[\exp(-t/\tau_{decay}) - \exp(-t/\tau_{buildup})]$, where we define the buildup rate as $\tau_{buildup}^{-1}$. The results are shown in Fig. 5 as a function of the average absorbed photon density at the surface of the crystal, $n_{ph}=\alpha N_{ph}/A$. Here, $N_{ph}$ is the number of photons in the laser pulse, $A$ is the illuminated surface area, and $\alpha$ is the wavelength-dependent absorption constant in rubrene. The reason for this choice of abscissa will become clear when we discuss the wavelength-dependent data, below.

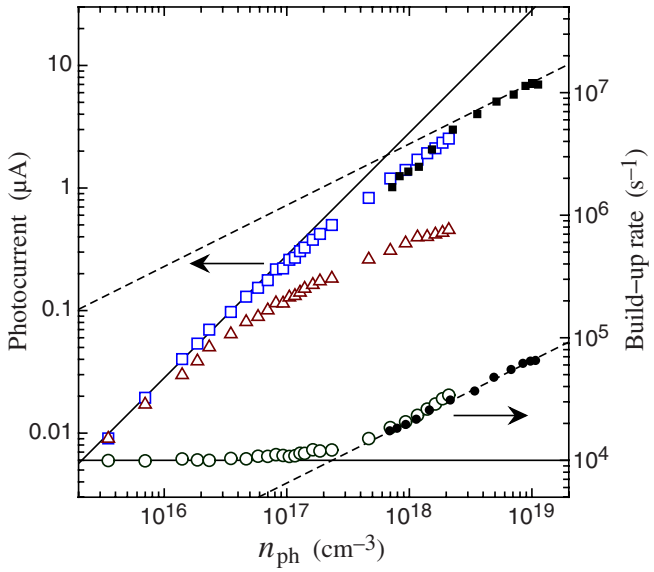


FIG. 5. (Color online) Photocurrent amplitude (open squares), buildup rate (open circles), and photocurrent integral (triangles) vs the average density of absorbed photons, as determined from the known absorption constant of rubrene and the energy density of the illuminating pulse. The photocurrent integral is the same data plotted in Fig. 4, normalized to the photocurrent amplitude scale for better visualization. The data were taken by varying the laser pulse energy at a fixed wavelength of 580 nm. Solid circles represent additional data points extending to higher photon densities obtained by varying the illumination wavelength at a fixed energy density of 3.5 $mJ/cm^2$. The solid lines correspond to the (linear) low-exposure limit, while the dashed lines represent a square-root dependence from the absorbed photon density.

We see that there is a very good agreement between the experimental power dependence that we observe for the photoinduced conductivity in rubrene and the behavior that we predicted in Fig. 2. Both the peak amplitude and the buildup rate deviate from their low-exposure behavior toward a square-root dependence from the energy density of the optical excitation. The buildup time of the photoconductivity starts to shorten near the same pulse energies where the photocurrent amplitude begins to saturate, as predicted in the presence of quadratic recombination.

To interpret our data, we now need to choose between the two possible cases where the quadratic-recombination model predicts this behavior of amplitude and buildup rate: the slow-photoexcitation case and the fast-photoexcitation case discussed in Sec II. As shown in Fig. 2, the two cases are distinguished by the amplitude of the final exponential relaxation, which starts saturating at lower exposures for the fast-photoexcitation case but does not saturate in the slow-

photoexcitation case. This will have a strong effect on the integral of the photocurrent, which is mostly determined by the amplitude of the final exponential relaxation at higher exposures, and it corresponds to what we observe in our data. Figure 5 shows that the photocurrent integral deviates from a linear dependence at exposures that are smaller by almost 2 orders of magnitude compared to the deviations observed for the peak photocurrent amplitude and the buildup rate. We thus conclude that in rubrene, the observed delayed photocurrent dynamics is in the fast-exposure regime, where the buildup time at low exposure coincides with the autoionization time of the intermediary state responsible for carrier generation, and the decay time is to be interpreted as a lifetime of the free carriers (the drift length always remains significantly shorter than the interelectrode spacing). This interpretation is also confirmed by our earlier experiments on the photoconductivity dynamics at higher powers,[17] where we could clearly see the typical signature of quadratic recombination in the time dynamics. It should also be noted that the simultaneously measured luminescence intensity remained linear with the exposure in this range of excitation energies.

We are therefore led to conclude that the intermediate reservoir state responsible for the delayed release of free carriers after short-pulse photoexcitation in the rubrene single crystal autoionizes after an average time of 100 $\mu$s to produce a free hole. Within our model, we cannot distinguish between an excitonic state that ionizes into free electrons and holes, with holes having the largest mobility and dominating the photoconductivity, and a defect state that interacts with an exciton to create a state that autoionizes into a free hole and a trapped electron. In both interpretations, the free electrons or the negatively ionized defect states have the same density as the free holes and lead to quadratic recombination, as described by our model. In fact, Fig. 5 shows that at higher pulse energies, the buildup dynamics starts being affected by the rate of geminate recombination. Both photocurrent amplitude and buildup rate trend toward a dependence from the square root of the population in the reservoir, as predicted in Sec. II. In this regime, we can therefore associate any change in the buildup time to a corresponding change in the initial reservoir population, which then depends linearly on the density of absorbed photons and on the energy density of the illumination.

An initial reservoir population that is linearly proportional to the number density of absorbed photons has several consequences for the interpretation of the buildup time at different wavelengths and at different temperatures. This will be the topic of the next two sections.

### B. Wavelength dependence

Since we established that the buildup time becomes proportional to the square root of the initial reservoir density and that the latter is proportional to the density of absorbed photons, we expect the buildup time at high enough exposures to become wavelength dependent because the absorption in rubrene varies strongly in the region between 500 and 600 nm.[17] The higher absorption of shorter wavelength light will lead to a larger density of absorbed photons close to the surface of the crystal. As an illustration, the absorption length in rubrene changes from $\sim$100 $\mu$m at 580 nm to $\sim$6 $\mu$m at 530 nm (for *b*-polarized light), corresponding to a more than 1 order of magnitude change in absorbed photon density and hence in the density of photoexcited excitons. Thus, it is possible to study the relationship between the effects of changing the illumination wavelength and the effects of changing the energy of the laser pulse at a fixed wavelength by plotting the parameters characterizing the photoconductivity as a function of the average absorbed photon density at the surface of the crystal, $n_{ph}=\alpha N_{ph}/A$, which we introduced above and which we chose as the abscissa of the plot in Fig. 5.

Wavelength dependence and power dependence are plotted together in Fig. 5. From the size of the illuminated area and the pulse energies used in the two experiments, it is possible to relate the two measurements in an absolute way. Even though we obtain a good agreement (to within 30%) when doing this for the buildup time, we preferred to slightly rescale the data we obtained in the wavelength-dependent measurement so that both the buildup time and amplitude determined at 580 nm correspond to the results obtained at 580 nm in the power dependence measurements.

The wavelength-dependence data in Fig. 5 neatly extends the power dependent data toward higher photon density while following exactly the same trend. The behavior of the buildup rate data is the expected one (following the predicted square-root dependence at higher photon densities), and it strongly reinforces our interpretation that the photoconductivity buildup in rubrene is determined by the dynamics of electron-hole recombination after ionization of the reservoir state. The behavior of the amplitude data, on the other hand, shows a continuing increase in amplitude even though the total number of absorbed photons remained the same while the wavelength was varied. This should not be the case for a constant number of absorbed photons if every photon absorption event has the same probability of filling a reservoir state. In other words, if the probability of a photoinduced exciton to "fill" a reservoir state did not depend on the distance from the surface at which the photon is absorbed, then we would expect a density of reservoir states that has a different depth distribution at different wavelengths but a total number of released carriers that remains the same or decreases because of quadratic recombination. This would lead to a photocurrent amplitude that slightly decreases at shorter wavelengths as the buildup rate increases, but this is not what we observe in Fig. 5.

A comparison of the wavelength dependence of the photocurrent buildup rate (dependent on density of excitation) and its amplitude (dependent on both total number of excitations and density) becomes the key to understanding the spatial distribution of the reservoir state. These data can be explained if the excitons are ionized efficiently into electron-hole pairs only within a short distance from the surface of the crystal. Only in this case does the total number of excitations contributing to the photoconductivity keep increasing with shorter wavelengths and shorter absorption lengths when keeping the number of photons in the illumination pulse constant. If only excitons created within a distance $L$ from the

surface are able to fill the reservoir state, then the total number of excitons contributing to the photoconductivity is proportional to $N_{ph}L$ as long as $L$ remains significantly smaller than the absorption length $1/\alpha(\lambda)$. The amplitude data in Fig. 5 can be explained in this way if $L<1/\alpha(530\ \text{nm}) \approx 6\ \mu\text{m}$. We note that in some other samples we investigated, we did indeed observe a decrease of the photocurrent amplitude toward the shorter wavelengths, as would be expected if those samples had an active region deeper than the 6 $\mu$m we estimate here.

The above observations and conclusions associate the intermediary state that is responsible for exciton ionization and ultimately the large photoconductivity of rubrene to an interaction of the photoexcited exciton with the surface of the crystal, either the surface itself or defect states only appearing close to the surface. The most probable candidate to explain this effect is the oxygen-induced defect previously observed at the surface of rubrene.[18,19] Upon interaction with this defect, the exciton would transform into a localized state that autoionizes into a free hole and a trapped electron. This is a relevant conclusion for heterojunction photovoltaic devices where the exciton does indeed ionize at the interface between two different materials, and it could also point the way to a new possibility for enhancing the exciton ionization probability. In the present case of photoexcitation in rubrene, both electron and hole remain inside the same material after ionization, and ionization takes a time of the order of 100 $\mu$s. In addition, the quantum efficiency for the generation of one free charge carrier from one absorbed photon appears to be extremely high in rubrene. Since we have shown that carrier photoexcitation happens efficiently only within a distance smaller than $\sim 5\ \mu$m from the surface, only less than about 6% of the photons are absorbed in the "active region" close to the surface (the absorption length for $b$-polarized light in rubrene is $\sim 100\ \mu$m at 580 nm). Counting only the photons absorbed in the active region and considering our earlier estimation of a lower limit of 0.01 for the quantum efficiency with which a photon is converted into a free carrier, one arrives at a minimum quantum efficiency of 0.16. However, the value of 0.01 would correspond to a drift length equal to the interelectrode spacing, which is certainly not the case because we did not observe any changes in the dynamics of the photocurrent up to an applied electric field of 3 kV/cm. Using the observed photocurrent decay time for the carrier lifetime, we estimate that the mobility of the photoexcited carriers has a maximum value of $2 \times 10^{-3}\ \text{cm}^2\ \text{V}^{-1}\ \text{s}^{-1}$, corresponding to a drift length of the order of $\sim 0.3$ mm at the 1.4 kV/cm field we used in our experiments. A drift length of the order of a fraction of a millimeter would be consistent with a quantum efficiency of 100%. Thus, our data imply an efficiency for the conversion between absorbed photon and free carrier that is practically of the order of unity at the surface of a rubrene crystal. This is indeed an extraordinary photogeneration efficiency.

The maximum value of the photocarrier mobility that we obtained above is much smaller than what was determined by measuring the field-effect mobility.[20] This can be explained from the fact that the field-effect measurement works with a larger number of injected carriers under trap filling conditions. In our case, the mobility of the photoexcited carriers is very probably trap limited, corresponding to the mobility of a hole that is trapped and thermally released multiple times in shallow trap levels such as those observed in Ref. 24 while it drifts in the valence band. This is not surprising because transport takes place at the oxidized surface of the crystal. Some more insights into this fact will be obtained from the temperature dependence of the photocurrent transients.

This conclusion of a quantum efficiency for photocarrier generation almost approaching unity is supported by the fact that we observed an absolute photoluminescence quantum efficiency of less than $\sim 2\%$ in an experiment where the photoexcitation was confined at the surface of a crystal. We obtained this estimation by comparing the integrated transient photoluminescence from rubrene powder obtained from naturally oxidized thin-plate crystals to that of a reference sample. This observation is consistent with a picture where the majority of molecular excitons created at the oxidized surface of rubrene fills the reservoir state responsible for the photoconductivity instead of radiatively recombining.

Under the assumption of unity quantum efficiency, we can estimate the upper limit for the number of carriers released in coincidence with the transition from the low-exposure to the high-exposure regime in Fig. 5. According to our model, this transition happens when $\gamma N_R(0) \approx w$, around the region where the buildup time shortens by a factor of 2. As seen from Fig. 5, the corresponding photon density is $10^{18}\ \text{cm}^{-3}$. This means that the corresponding $N_R(0)$ is at least equal to this value. Since we know that $w=10^4\ \text{s}^{-1}$ because we assigned $w$ to the low-exposure buildup rate, we can derive a lower limit for the quadratic-recombination constant $\gamma_{MIN} = 10^{-14}\ \text{cm}^3\ \text{s}^{-1}$. We need $\gamma$ to be at least this large in order to explain the saturation behavior of the photocurrent that we have seen. We note that if the mobility of the carriers is trap limited, as mentioned above, and if the recombination occurs at negatively ionized reservoir states, the constant $\gamma$ does not necessarily reflect the recombination process of a free hole and a free electron.

### C. Dependence on temperature

In order to obtain even more information on the mechanism of reservoir filling and ionization, we investigated the sensitivity of the photoconductivity dynamics on the temperature. In this respect, it is important to reiterate that the buildup rate of the photoconductivity is determined by two different effects in the low- and in the high-exposure limit. In the high-exposure limit, it is a sensitive measurement of the amount of filled reservoir states $N_R(0)$, which is proportional to the square of the buildup rate because of quadratic recombination. In the low-exposure limit, on the other hand, the buildup rate is determined by the ionization rate of the reservoir state and it does not depend on photoexcitation density.

The temperature dependence of the buildup rate in the high-exposure regime is thus a unique opportunity to get information on the temperature dependence of the process that leads from an absorbed photon to the intermediary state responsible for the release of charge carriers in rubrene. Nor-

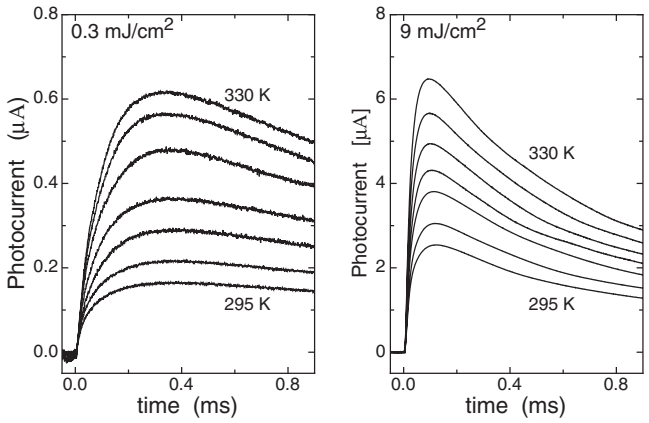


FIG. 6. Photoconductivity traces obtained in the temperature range 295–330 K by varying the temperature in steps of 5 K. The traces were measured in the low-exposure limit (0.3 mJ/cm$^2$) (left) and in the high-exposure limit (9 mJ/cm$^2$) (right).

mally, one could not extract such an information from just the photoconductivity amplitude because its temperature dependence is determined both by the variation in the number carriers and by the temperature dependence of the mobility.

Figure 6 shows transient photoconductivity measurements performed in the temperature range from 295 to 330 K both in the low-exposure regime and in the high-exposure regime. Figure 7 shows the corresponding temperature dependence of the buildup rate and of the photocurrent amplitude. Because of the proportionality between the square of the buildup rate and the reservoir density that we expect in the high-exposure limit [we showed in the previous section that the square of the build up rate in the high-excitation limit is given by $\gamma N_R(0)w$], we plotted the square of the buildup rate in Fig. 7. Even though we chose to use only a limited temperature interval—in order to avoid permanent changes to the crystal and to the contacts due, e.g., to oxidation—we notice that the buildup rate increases slightly but significantly with temperature when it is measured in the high-excitation regime, while it does not do so and instead remains practically constant when it is measured in the low-excitation regime (the larger scatter of the buildup rate data under low-excitation conditions is caused by the small signal to noise ratio). The low-exposure data show that the rate of ionization of the reservoir state—which is responsible for the photoconductivity buildup time for small excitation energies—does not change significantly in this limited temperature range. On the other hand, the other quantities plotted in Fig. 7 show a clear temperature dependent trend. We can compare the relative temperature dependences of the various quantities by using the slope of the data in Fig. 7, which directly gives a measure of an "activation energy" $E_a$ appearing in a temperature dependence of the form $\exp(-E_a/k_BT)$. From Fig. 7, one can read $E_a \sim 0.2 \pm 0.02$ eV for the square of the photoconductivity build up rate [proportional to $N_R(0)\gamma$] and $E_a \sim 0.4 \pm 0.02$ eV for the amplitude of the photocurrent measured at low excitation [proportional to $\mu N_R(0)$]. On the other hand, the amplitude of the photocurrent measured at high excitation (proportional to $\mu\sqrt{wN_R(0)/\gamma}$) can be described by an activation energy of

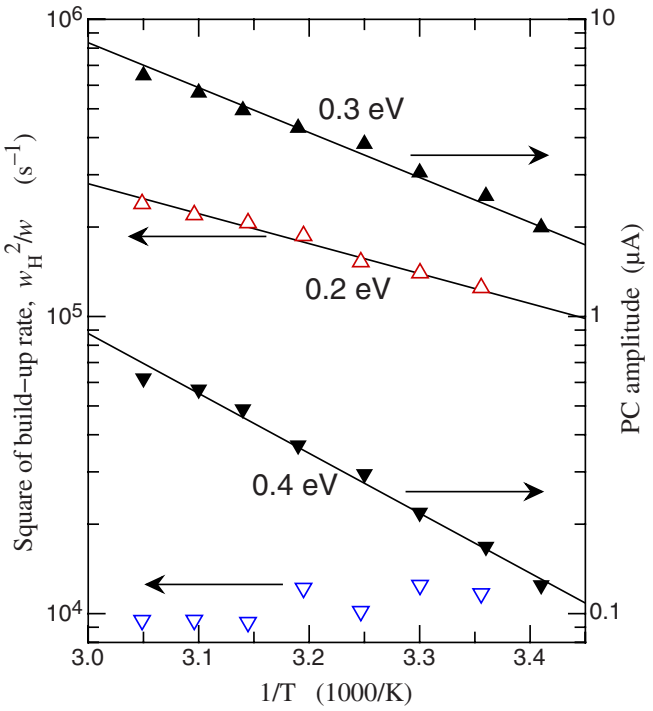


FIG. 7. (Color online) Photocurrent amplitude (full triangles) and square of buildup rates (empty triangles) vs reciprocal temperature at low and at high exposures. The low- and the high-exposure data are represented by the triangles pointing down and up, respectively. The square of the buildup rate $w_H$ is normalized by dividing it by the buildup rate at room temperature and low exposure, $w = 10^4$ s$^{-1}$, and the model predicts that it tends to $\gamma N_R(0)$ at high exposure. The solid lines are Arrhenius-like temperature dependences, with the labels indicating the corresponding activation energies.

$0.3 \pm 0.02$ eV. It is interesting that the difference in activation energy between the low-exposure and the high-exposure case for the temperature dependence of the photocurrent amplitude is one-half of the activation energy we get from the square of the buildup rate. This is expected from our model because the ratio of the photocurrent amplitude in the two limits is proportional to $\sqrt{\gamma N_R(0)}$ (the mobility drops out), while the square of the buildup rate in the high-exposure limit is proportional to $\gamma N_R(0)$. If the three fundamental quantities $\mu$, $\gamma$, and $N_R(0)$ that determine the photocurrent response are also assumed to have a temperature dependence of the kind $\exp(-E_a/k_BT)$, the data imply that the sum of the activation energies for $N_R(0)$ and for $\mu$ must be of the order of 0.4 eV, while the difference of the activation energies for $\mu$ and $\gamma$ must be of the order of 0.2 eV. This could be consistent with a quadratic-recombination constant $\gamma$ that is temperature independent in the temperature interval we studied, while both mobility and reservoir density are activated with an energy of ~0.2 eV. In the absence of more data, this choice seems to be the simplest one, explaining all the temperature dependent data by a mobility and a reservoir density that change with temperature as if they had an activation energy of 0.2 eV. This energy corresponds approximately to the energy of the carbon-carbon vibration in the rubrene molecule and to the energetic distance between the vibrational

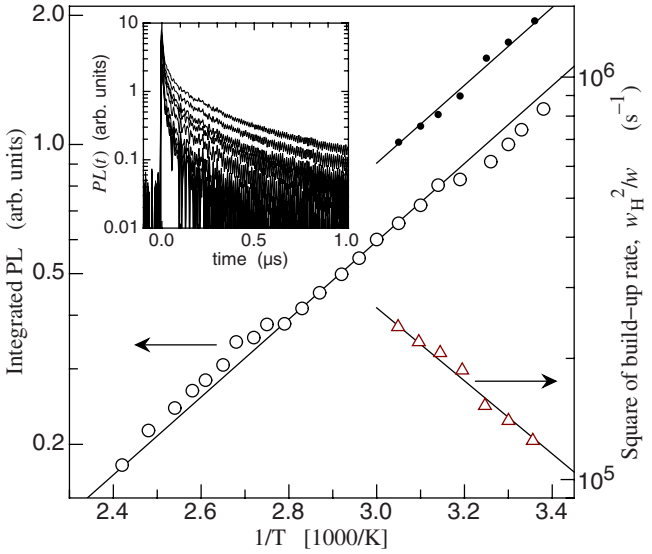


FIG. 8. (Color online) Time integral of the photoluminescence vs reciprocal temperature (open circles). The photoluminescence transients from which the data were collected are given in the inset, showing a clear shortening of the microsecond decay for higher temperatures. The data in the inset are given in the temperature range 295–415 K with a step of 15 K. The data were obtained at an excitation wavelength of 570 nm and monitoring at $620 \pm 10$ nm. The white triangles give the square of the buildup rate at high exposure, which is proportional to $\gamma N_R(0)$ and is the same data already plotted in Fig. 7. The solid dots are the reciprocal of these data, which we plot in arbitrary units to highlight the parallelism with the temperature dependence of the photoluminescence.

levels observed, e.g., in the absorption spectrum of rubrene crystals.[17] In addition, this energy is also similar to the depth of the acceptor level identified in oxidized crystals in Refs. 19 and 24, which reinforces both the above interpretation of the temperature dependence and our earlier conclusion that molecular excitons interact with oxygen-induced defect states to ultimately ionize and generate free charge carriers.

Thus, the temperature-induced changes in the photoconductivity dynamics both at low excitation and at high excitation are consistent with the interpretation that the density of reservoir states, $N_R(0)$, grows with temperature near room temperature, increasing by 50% for a 10% change in temperature. We now show that these temperature dependences are also accompanied by a similar temperature dependence of the photoluminescence. We have shown earlier[17] that the primary excitation that is responsible for the ultimate release of charge carriers in rubrene is the same molecular exciton that is also responsible for the photoluminescence. We have also shown earlier[17] that the photoluminescence in the high-exposure regime shows a slower decay with a time constant of 1 $\mu$m after a fast initial transient. We now investigated the temperature dependence of this luminescence and found that the decay becomes faster at higher temperatures. Numerically, this is best expressed as the temperature dependence of the time integral of the photoluminescence signal. The results are plotted in Fig. 8. We monitored the photoluminescence close to its maximum at 618 nm (Ref. 17) using a bandpass filter centered at $620 \pm 10$ nm. From the decrease in the time integral of the photoluminescence transient, we extract an activation energy for the temperature quenching of $0.18 \pm 0.02$ eV that is very close to the 0.2 eV we estimated from the temperature dependence of the photocurrent dynamics in a limited temperature interval, and that we assigned to the temperature dependence of the initial reservoir density $N_R(0)$. Thus, as the radiative recombination on the submicrosecond time scale decreases, the number of states responsible for the photocurrent increases proportionally. The increase in the population of reservoir states is correlated to a quenching of the exciton luminescence. This does not necessarily mean that the decay of the luminescence is directly related to the filling of the reservoir state $N_R(0)$, but it may point at a common origin of the two effects.

In the above discussion, we argued that the reservoir state could be related to the oxygen-induced defect identified in Refs. 18 and 19 and also observed in Ref. 24. In this respect, it is important to underline that Ref. 19 argued that an oxygen-induced defect could be responsible for the luminescence emitted close to the surface. The above data show, however, that the source of the transient photoluminescence and the reservoir state responsible for delayed photoconductivity cannot be the same state. First, because photoluminescence and reservoir density have an opposite temperature dependence, and second, because the photoluminescence disappears in the submicrosecond scale, while the photocurrent arises at longer times. This is but one example of the open questions that will need to be resolved with additional experiments in the future.

## IV. CONCLUSIONS

Our combined analysis of short-pulse induced photocurrent and photoluminescence transients and, in particular, their dependence on pulse energy, pulse wavelength, and temperature allowed us to identify several main features of the charge carrier photoexcitation process in the rubrene molecular crystal.

We found that molecular excitons photoexcited close to the surface of the rubrene crystal transform within a microsecond from the time of their creation into an intermediary state that ionizes into free charge carriers over a lifetime of $\sim 100$ $\mu$s. This delayed emission of charge carriers happens only within a depth of the order of micrometers from the crystal surface, but it has a quantum efficiency for the conversion of an absorbed photon into a free charge carrier that may become quite close to unity. This explains the large photoconductivity that is observed in rubrene crystals.

To arrive at this conclusion, we developed a model taking into account the delayed excitation of charge carriers after short-pulse excitation that is generally applicable to several pulsed photoconductivity experiments and takes into account the effects of quadratic recombination. The model explains all the peculiarities of the photocurrent dynamics in rubrene, from the delayed onset of the conductivity to the shortening of the buildup dynamics and the amplitude saturation observed at higher light intensities and shorter wavelengths, which can both be understood on the grounds of the absorbed photon density. Our analysis could successfully ex-

ploit the properties of the delayed photoexcitation dynamics of rubrene to extract information from, e.g., the variations of the photocurrent buildup time in the various photoexcitation regimes. Such information would otherwise not be available from experiments performed under continuous illumination.

The delayed photoconductivity that is observed after pulsed excitation in rubrene is a quite uncommon situation, and we are not aware of other materials where such an effect has been seen. However, its clearly delayed onset and strong magnitude make it clear—at least for the range of absorbed photon densities and wavelengths that we investigated—that this delayed photoconductivity dominates any charge carrier generation that may take place while the illuminating pulse is present in the crystal. The fact that our direct electric experiments do not reveal any significant instantaneous generation of charge carriers at low exposure is not in agreement with the observations of a signal assigned to free carriers that appeared within a picosecond from photoexcitation in Ref. 6. For the moment, this discrepancy can only be reconciled by assuming that what is observed in Ref. 6 is the result of the immediate ionization of a fraction of the photoexcited excitons, while the rest of photoexcited excitons follow the delayed path to charge carrier generation that we outlined above. The current due to the fraction of carriers that are immediately photoexcited must be relatively small and does not give a detectable effect, in our low-exposure experiments, while its contribution may become stronger at higher exposures and shorter wavelengths, where the amplitude of the delayed contribution saturates. In any case, it is interesting to note that the signal associated with an instantaneous creation of free charge carriers in Ref. 6 is the smallest for rubrene among a family of related materials.

Finally, we come back to the discussion of the origin of the intermediary reservoir state that is responsible for the delayed photoconductivity in rubrene, and that we found can be formed only in a surface layer with a thickness of the order of some micrometers, a thickness that may well be sample dependent. While further investigations are clearly necessary in order to better identify its origin, we suggested that this state may be related to the same oxygen-induced defects that have recently been identified in Refs. 18, 19, and 24. We do not consider the presence of this oxidized layer in rubrene an undesirable property. On the contrary, we estimated that photoexcitation of free charge carriers by visible light can happen with almost 100% quantum efficiency in this oxidized layer. This explains the large photosensitivity of rubrene, including the sensitive optical switching of a field-effect transistor at the surface of a crystal.[18] In addition, it is also possible to envisage the application of this unique effect toward obtaining efficient harvesting of light energy in the visible spectral range, without the need of heterostructures to ensure that photoexcited excitons are ionized, which is otherwise a common challenge in organic materials for photovoltaic applications.

## ACKNOWLEDGMENTS

Acknowledgment is made to the donors of the American Chemical Society Petroleum Research Fund for support of this research at Lehigh (45741-AC10) and to the National Science Foundation for support of the work at Rutgers (Grants No. DMR-0405208 and No. ECS-0437932).

[1] M. Pope and C. Swenberg, Annu. Rev. Phys. Chem. **35**, 613 (1984).
[2] M. Pope and C. Swenberg, *Electronic Processes in Organic Crystals and Polymers* (Oxford University Press, New York, 1999).
[3] E. Silinsh and V. Capek, *Organic Molecular Crystals: Interaction, Localization and Transport Phenomena* (American Institute of Physics, New York, 1994).
[4] F. A. Hegmann, R. R. Tykwinski, K. P. H. Lui, J. E. Bullock, and J. E. Anthony, Phys. Rev. Lett. **89**, 227403 (2002).
[5] O. Ostroverkhova, D. G. Cooke, S. Shcherbyna, R. Egerton, F. A. Hegmann, R. R. Tykwinski, and J. E. Anthony, Phys. Rev. B **71**, 035204 (2005).
[6] O. Ostroverkhova, D. G. Cooke, F. A. Hegmann, J. E. Anthony, V. Podzorov, M. E. Gershenson, O. D. Jurchescu, and T. T. M. Palstra, Appl. Phys. Lett. **88**, 162101 (2006).
[7] E. Hendry, J. M. Schins, L. P. Candeias, L. D. A. Siebbeles, and M. Bonn, Phys. Rev. Lett. **92**, 196601 (2004).
[8] R. Kersting, U. Lemmer, M. Deussen, H. J. Bakker, R. F. Mahrt, H. Kurz, V. I. Arkhipov, H. Bässler, and E. O. Göbel, Phys. Rev. Lett. **73**, 1440 (1994).
[9] I. B. Martini, A. D. Smith, and B. J. Schwartz, Phys. Rev. B **69**, 035204 (2004).
[10] D. Moses, H. Okumoto, C. H. Lee, A. J. Heeger, T. Ohnishi, and T. Noguchi, Phys. Rev. B **54**, 4748 (1996).
[11] *The Nature of Photoexcitations in Conjugated Polymers*, edited by N. S. Sariciftci (World Scientific, Singapore, 1997).
[12] B. J. Schwartz, Annu. Rev. Phys. Chem. **54**, 141 (2003).
[13] F. Cordella, R. Orru, M. A. Loi, A. Mura, and G. Bongiovanni, Phys. Rev. B **68**, 113203 (2003).
[14] A. Davydov and A. Serikov, Phys. Status Solidi B **44**, 127 (1971).
[15] A. Matsui, J. Opt. Soc. Am. B **7**, 1615 (1990).
[16] Y. Toyozawa, in *Proceedings of the International Symposium on Organic Materials*, edited by P. Reineker, H. Haken, and H. Wolf (Springer, Berlin, 1983), p. 90.
[17] H. Najafov, I. Biaggio, V. Podzorov, M. F. Calhoun, and M. E. Gershenson, Phys. Rev. Lett. **96**, 056604 (2006).
[18] V. Podzorov, V. Pudalov, and M. Gershenson, Appl. Phys. Lett. **85**, 6039 (2004).
[19] O. Mitrofanov, D. V. Lang, C. Kloc, J. M. Wikberg, T. Siegrist, W.-Y. So, M. A. Sergent, and A. P. Ramirez, Phys. Rev. Lett. **97**, 166601 (2006).
[20] V. Podzorov, E. Menard, A. Borissov, V. Kiryukhin, J. A. Rogers, and M. E. Gershenson, Phys. Rev. Lett. **93**, 086602 (2004).
[21] G. Montemezzani, P. Rogin, M. Zgonik, and P. Günter, Phys. Rev. B **49**, 2484 (1994).
[22] P. Bernasconi, G. Montemezzani, I. Biaggio, and P. Günter, Phys. Rev. B **56**, 12196 (1997).

[23] R. de Boer, M. Gershenson, A. Morpurgo, and V. Podzorov, Phys. Status Solidi A **201**, 1302 (2004).
[24] C. Krellner, S. Haas, C. Goldmann, K. P. Pernstich, D. J. Gundlach, and B. Batlogg, Phys. Rev. B **75**, 245115 (2007).
[25] For the sake of completeness, we also give a full version of Eq. (12) that is valid in the case when a density of holes $p(0)$ is photoexcited instantaneously [in our treatment we otherwise always assumed $p(0) \ll N_R(0), N_T, p(t)$]. Such an instantaneous photoexcitation may happen if there is a finite probability that delocalized holes are created immediately upon photoexcitation.[6] $p(0)$ then appears as an initial condition together with $N_R(0)$ and it gives rise to the following evolution in the fast-photoexcitation case:

$$p(t) = \frac{p(0)e^{-\gamma_T N_T t} + N_R(0)[e^{-\gamma_T N_T t} - e^{-wt}]}{1 + H(t) - G(t) + K(t)},$$

where $K(t) = p(0)\gamma\gamma_T^{-1}N_T^{-1}[1 - \exp(-\gamma_T N_T t)]$.